Mechanical and Surface Properties of Chemical Vapour Deposited Protective Aluminium Oxide Films on TA6V Alloy

D. Samélor[1,a], M. Aufray[1,b], L. Lacroix[2,c], Y. Balcaen[2,d], J. Alexis[2,e], H. Vergnes[3,f], D. Poquillon[1,g], J-D. Beguin[2,h], N. Pébère[1,i], S. Marcelin[1,j], B. Caussat[3,k], C. Vahlas[1,l]

[1] Centre Interuniversitaire de Recherche et d'Ingénierie des Matériaux (CIRIMAT)

ENSIACET, 4 allée Emile Monso, BP 44362, 31432 Toulouse Cedex 4, France

[2] Ecole Nationale d'Ingénieurs de Tarbes (ENIT), 47, avenue d'Azereix, BP 1629, 65016 Tarbes, France

[3] Laboratoire de Génie Chimique (LGC)

ENSIACET, 4 allée Emile Monso, BP 84234, 31432 Toulouse Cedex 4, France

[a] diane.samelor@ensiacet.fr, [b] maelenn.aufray@ensiacet.fr, [c] loic.lacroix@enit.fr, [d] yannick.balcaen@enit.fr, [e] joel.alexis@enit.fr, [f] hugues.vergnes@ensiacet.fr, [g] dominique.poquillon@ensiacet.fr, [h] jean-denis.beguin@enit.fr, [i] nadine.pebere@ensiacet.fr, [j] sabrina.marcelin@ensiacet.fr, [k] brigitte.caussat@ensiacet.fr, [l] constantin.vahlas@ensiacet.fr

Keywords: MOCVD, amorphous alumina, process modelling, mechanical properties, oxidation resistance, corrosion resistance, wetting.

Abstract. Mechanical, barrier and surface properties of aluminium oxide films were investigated by nanoindentation, microscratch and micro tensile tests, by isothermal oxidation and voltammetry, and by contact angle measurement. The films were grown on TA6V substrates by a low pressure MOCVD process from aluminium tri-isopropoxide. Modelling of local gas flow, gas concentration and deposition rate profiles was performed using the CFD code Fluent on the basis of an apparent kinetic law. Films grown at 350 °C are amorphous AlO(OH), the one at 480 °C is amorphous Al_2O_3 and the one at 700 °C is nanocrystalline γ-Al_2O_3. Scratch tests and micro tensile tests resulted in adhesive failure on the two films grown at low temperature whereas cohesive failure was observed for the high temperature growth. Sample processed at 350 °C presents significantly lower oxidation kinetics in dry air than the bare substrate. Contact angle changes approximately from 100 to 50 degrees for films processed at 350-480 °C and 700 °C, respectively. Concerning the electrochemical behavior in NaCl environment, polarization curves revealed that amorphous alumina coatings improved the corrosion resistance by comparison with the others oxide films. These consolidated results reveal promising combination of properties for the films grown at different temperatures with regard to the targeted applications.

Introduction

Titanium alloys have been largely developed for aeronautical components like turboshaft engines, because of their good specific mechanical resistance, their high tenacity and their structural stability. However, under severe conditions, the combined effects of high temperature, heavy mechanical stress and oxidizing and corrosive environment can reduce the mechanical performance and ultimately lead to premature failure of the coated parts. Over recent years a variety of protective coatings have been developed for hot sections engines. These coatings must be thermo-mechanically and chemically compatible with the substrate. Previous studies revealed the beneficial effect of alumina (Al_2O_3) forming alloys for the hot corrosion resistance in chlorine-containing environments [1]. However, the characteristics of such thermally developed alumina scales are not necessarily compatible with the corresponding specifications. For example, the microstructure of such scales is often neither flat nor smooth. Consequently these oxides may not efficiently serve as

oxidation barrier unless they are engineered in a narrow parametric window. Even in this case, the formation of the desired phases, such as α-alumina; i.e. the terminal allotrope of aluminium oxide may not be accessible in acceptable conditions. Alternatively, if such protective coatings can be brought on the surface by an external means such as a deposition process then, their characteristics can be engineered with regard to the desired properties without the constraints imposed by the substrate. However, in this case particular constraints should be tackled such as the adhesion to the substrate or the conformal coverage of the part.

During the last years, a chemical vapour deposition process (CVD) has been investigated by the authors for the application of aluminium oxide protective coatings on commercial titanium alloys such as Ti6242 and TA6V [2-8]. The use of CVD is being justified by the high throwing power and by the possibility this technique provides to conformally cover complex-in-shape substrates. The investigated process involves the use of a metalorganic (MO) precursor, namely aluminium tri-isopropoxide (ATI). Advantages of the MOCVD technique is the operation at low to moderate temperature and particularly the use of ATI allows operating in the absence of additional oxygen source.

The mechanical and physicochemical properties of such coatings are being investigated in the frame of an ongoing project. Preliminary results are reported in this contribution. First, information on the processing conditions will be presented together with the applied techniques for the determination of the properties of use of the material. These are electrochemical measurements, contact angle measurements, high temperature oxidation and mechanical tests namely nanoscratch and nanoindentation. The CVD process is modelled in terms of fluid flow and gas composition profiles and is based on a global kinetic scheme for the dissociation of ATI. The outcome of this modelling will be presented, followed by the results on the characterization of the properties of the coatings.

Experimental and theoretical tools

The aluminium oxide films were obtained by MOCVD from ATI. The process was described in [9]. It can be recalled that deposition experiments were performed in a horizontal hot-wall reactor with an internal diameter of 26 mm, at low pressure in the temperature range 350 °C to 700 °C with nitrogen as the carrier gas. The coatings were deposited on TA6V substrates polished down to 4000 grade with SiC paper. Tensile specimens or 10 mm*15 mm rectangular samples were used, as a function of the targeted characterizations. 10 mm*15 mm silicon substrates were also used for the determination of the apparent kinetic law.

The characteristics of the obtained films were previously reviewed and it was mentioned that composition, microstructure and crystallinity of the films can be adjusted by varying the processing conditions [5]. It was confirmed that films processed at 350 °C are amorphous and composed of aluminium oxyhydroxide, AlOOH. Those processed at 480 °C and at 700 °C are composed of Al_2O_3, respectively amorphous and nanocrystalline. Tables 1 and 2 resume the experimental conditions and the characteristics of the obtained films for the study of coating properties (table 1) and the establishment of the apparent kinetic law (table 2).

Table 1: Processing conditions for the alumina coatings and characteristics of the obtained films

Sample code	$T_{deposition}$ [°C]	Q_{total} [sccm]	$Q_{N2, ATI}$ [sccm]	P_{ATI} [Torr]	P [Torr]	Composition
C700	700	651.5	20	0.01	5	nanocrystalline Al_2O_3
B480	480					amorphous Al_2O_3
A350	350					amorphous AlO(OH)

Films morphology was investigated by scanning electron microscopy with a JEOL 7000F SEM FEG instrument, equipped with a SDD 129eV BRUCKER X-ray dispersive spectroscopy analyzer. Their electrochemical behavior was characterized by voltammetry (anodic and cathodic polarization curves). A three-electrode cell was used for the experiments: the coated TA6V coupons as working

electrode, a saturated calomel reference electrode (SCE) and a platinum grid as auxiliary electrode. Experiments were performed in a 0.1 M NaCl solution at room temperature without stirring. The polarization curves were obtained after 1 h of immersion at the corrosion potential from cathodic to anodic potentials. The potential sweep rate was fixed at 0.277 $mV.s^{-1}$.

Table 2: Processing conditions for the determination of the kinetic parameters

Sample code	$T_{deposition}$ [°C]	Q_{total} [sccm]	$Q_{N2, ATI}$ [sccm]	P_{ATI} [Torr]	P [Torr]
E1	480	651.5	20	0.01	5
E2				0.025	

The contact angles were measured using a Digidrop Contact Angle Meter from GBX Scientific Instruments. The protocol used consists in depositing a liquid drop of an accurately known volume (3–5 µL, controlled with a needle with a 0.41 mm internal diameter) on the surface of the sample and then measuring the static contact angle (θ). In the present study, a few seconds were sufficient to obtain stabilization of the interfacial forces and thus, the static contact angle was measured just after deposition of the liquid drop. In order to assess the homogeneity of the surface properties, 12 measurements were performed on 6 drops deposited at different locations on the samples and the average contact angle was calculated. Ultra-pure water (resistivity >18 MOhm) was used as probe liquid for the droplets to evaluate the hydrophilic behaviour of the surface. All the experiments were performed at room temperature.

High temperature oxidation tests were conducted in a SETARAM TAG24S instrument at 600 °C. This apparatus combines good accuracy with limited buoyancy effects due to a symmetrical furnace in which an inert sample counterbalances such effects. Isothermal oxidation tests were carried out in 1 atm flowing synthetic air (80% N_2, 20% O_2). Heating and cooling rates were one degree per second. Hold time was 100 h. The weight gain was continuously measured as a function of time. Only sample A350 was tested up to now. Before test, the surface area of the sample was determined. Then it was ultrasonically cleaned in acetone and ethanol and finally dried. The sample was weighted before and after the oxidation test using a Sartorius balance (±10µg). Oxidation kinetics during isothermal tests was analyzed following the procedure detailed in [10].

The nanoindentation tests were carried out with the nanoindentor XP from MTS. A matrix of 20 measurements in dynamic mode was carried out on each film by imposing a maximum depth of 300 nm. The hardness of materials is defined as the ratio between normal force and projected contact area. The elastic modulus E was estimated from the slope at the beginning of the unloading curve which was computed by fitting this curve to a power law as suggested by Oliver and Pharr [11]. The practical adhesion was determined by scratch tests (standard EN 1071) and microtensile tests [12].

Process modelling: theory and results

The commercial code Fluent (www.ansys.com/products/fluid-dynamics/fluent/) was used to calculate the local gas flow and gaseous species molar fractions considering the following apparent chemical reaction which takes into account the tetrameric structure of ATI in the vapour phase as discussed in [4] and [8]:

$$[Al(OC_3H_7)_3]_4 \rightarrow 2\ Al_2O_3 + 12\ C_3H_6 + 6\ H_2O \quad (1)$$

A 3D geometrical domain of 56.341 meshes was built up to represent the reactor. Phenomena were assumed to occur in steady-state and in laminar conditions (Reynolds number lower than 1000). The experimental thermal profile in central position along the reactor length was considered for these calculations.

Morssinkhoff [13] has shown that deposition rate R_{si} (kg/m^2s) of alumina from ATI can be represented by the following apparent kinetic law:

$$R_{si} = k_0 * \exp(-E_a/RT) * [ATI]^n \quad (2)$$

where k_0 is a pre-exponential constant, E_a (J/mol) an activation energy, T (K) the temperature and n the apparent reaction order. This law was adopted in the present study for the establishment of the apparent kinetic model.

The central zone of the MOCVD reactor; i.e. the region where the substrates were disposed was virtually divided into a series of perfectly mixed cylindrical reactors of 1 cm in length. The alumina deposition rate was supposed to be uniform in each compartment. In these conditions, the following mass balance was written for ATI:

$$Q_{i-1} * y_{i-1} - Q_i * y_i = \pm R_{si} * S_i \quad (3)$$

where Q_i ($kg.s^{-1}$) is the total gaseous mass flow rate and y_i the mass fraction of ATI in the i^{th} compartment. Q_i was calculated along the CVD reactor by considering the mass of deposited aluminium oxide. The inlet ATI mass fraction in the first compartment was taken equal to that provided by the bubbler at the reactor inlet. The gas flow is supposed to be saturated at the exit of the bubbler. The saturation vapour pressure is equal to [8]:

$$\log_{10} P_{ATI} = 11.35 - 4400/T \quad (4)$$

where P_{ATI} is the partial pressure of ATI in Pa and T is the temperature of the bubbler in K.

By minimizing the error between the experimental deposition rate R_d of aluminium oxide and the calculated one R_{si} for the three runs, the Excel software was finally used to determine the kinetic parameters k_0, E_a and n. The obtained values are: $k_0 = 1.5\ 10^6\ kg.m^{2.5}/(mol^{1.5}s)$, $E_a = 78.1$ kJ/mol and n = 1.5.

Hofman et al. [14] determined an apparent activation energy of 30 kJ/mol and a second order dependence in ATI at 3 Torr between 230 °C and 440 °C. In the present work both processing temperature and pressure are higher; probably leading to different deposition mechanisms. This could explain the observed shift of results.

These kinetic parameters were finally implemented into Fluent to simulate the CVD reactor in steady state conditions. Figure 1 presents the comparison between the experimental and calculated deposition rates radially averaged along the reactor axis, for runs E1 and E2 (bubbler temperature respectively equal to 100 and 110°C, and inlet ATI partial pressure being calculated using relation (4)). The model offers a convenient representation of the deposition rate for the two runs, especially near the entrance zone. It is likely that after the first 0.2 m, the deposition mechanisms are different, probably due to homogeneous reactions. The average relative error between the two sets of results for the two runs is lower than 20% which is acceptable considering (i) the discrepancies of MOCVD experiments, (ii) the assumption of the saturation of the input gas with the precursor vapours and, most importantly (iii) the fact that the adopted kinetic law is only apparent.

Coatings properties

Voltammetry. The polarization curves obtained for the three different films deposited on TA6V are presented in Fig. 2. The values of the corrosion potential are approximately the same independently of the coating. For the three samples, the anodic current density progressively increases as the potential increases. Sample B480 presents the lowest cathodic and anodic current densities. Thus, amorphous Al_2O_3 insulating coatings allow an improvement of the corrosion resistance. Amorphous AlO(OH) coatings (A350) provide limited corrosion protection attributed to their lamellar nanostructure and to the presence of reactive hydroxo groups. The crystallized alumina containing coatings (C700) provide intermediate corrosion protection probably due to the presence of grain boundaries which favor electrolyte penetration through the film.

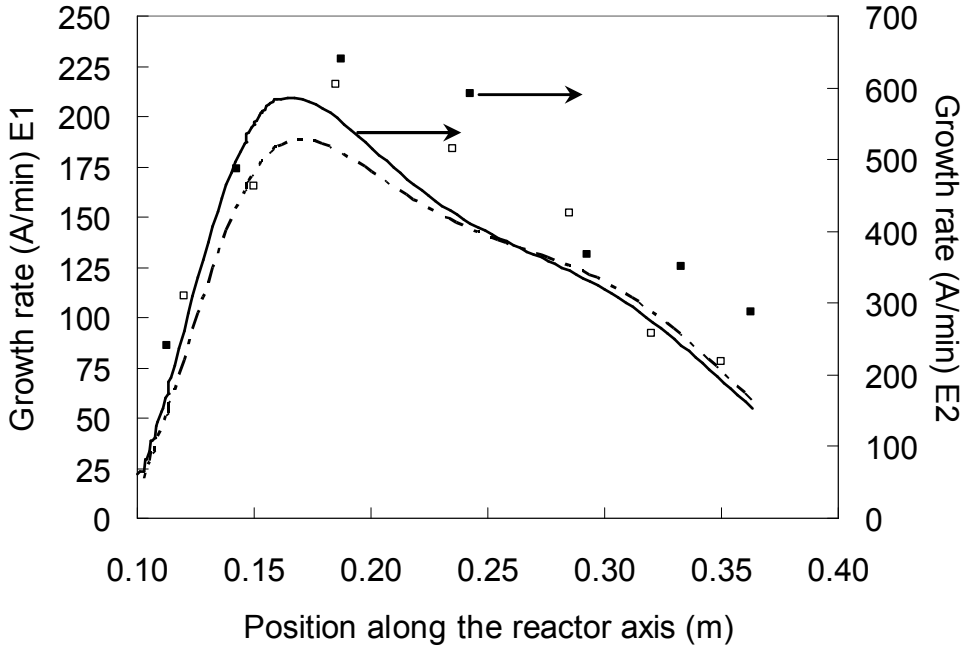

Fig. 1. Comparison between the experimental and the calculated deposition rates evolution along the reactor axis for runs E1 and E2 (□: experimental growth rate E1, ■ experimental growth rate E2, ----: model growth rate E1, —: model growth rate E2). Error bars for the experimental results are limited by the size of the squares.

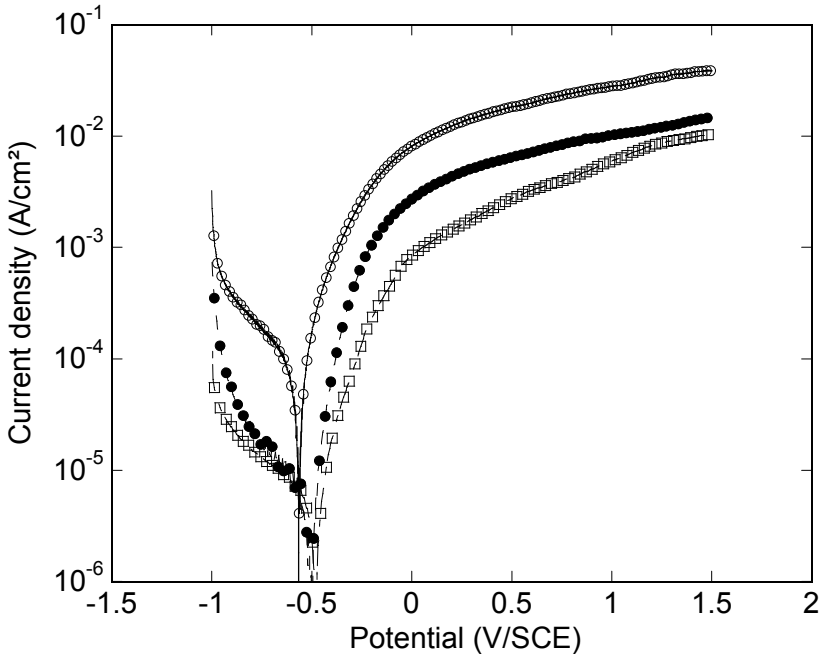

Fig. 2. Polarization curves for the three different aluminum oxide coatings plotted from cathodic to anodic potentials in 0.1 M NaCl solution (○: A350, □: B480, ●: C700)

Wetting. Table 3 shows measured contact angle of water drops on various substrates. The contact angles increase with the deposition temperature showing that amorphous surfaces are hydrophobic whereas the crystalline surface is hydrophilic.

Oxidation. In order to quantify the protective efficiency of the coating, an uncoated sample was oxidized in the same conditions: Fig. 3 compares oxidation kinetics of both the uncoated and the A350 samples. Net mass gain is plotted versus the square root of time in order to check that oxidation kinetics is parabolic after 10 hours of oxidation. The oxidation kinetics of the uncoated

sample follow a parabolic law with oxidation kinetics rate of 4.6 10^{-8} $mg^2.s^{-1}.cm^{-4}$. This value is in good agreement with the data available in literature for pure titanium [15, 16] and Ti-4.02wt%Al [17]. The coated sample A350 has a lower oxidation kinetics 1.1 10^{-8} $mg^2.s^{-1}.cm^{-4}$. This result need to be confirmed but are quite promising.

Table 3: Wetting properties of the coatings

Sample code	Contact angles	Surface behaviour
C700	47.8±3.3	hydrophilic
B480	106.0±2.4	hydrophobic
A350	103.3±1.0	hydrophobic

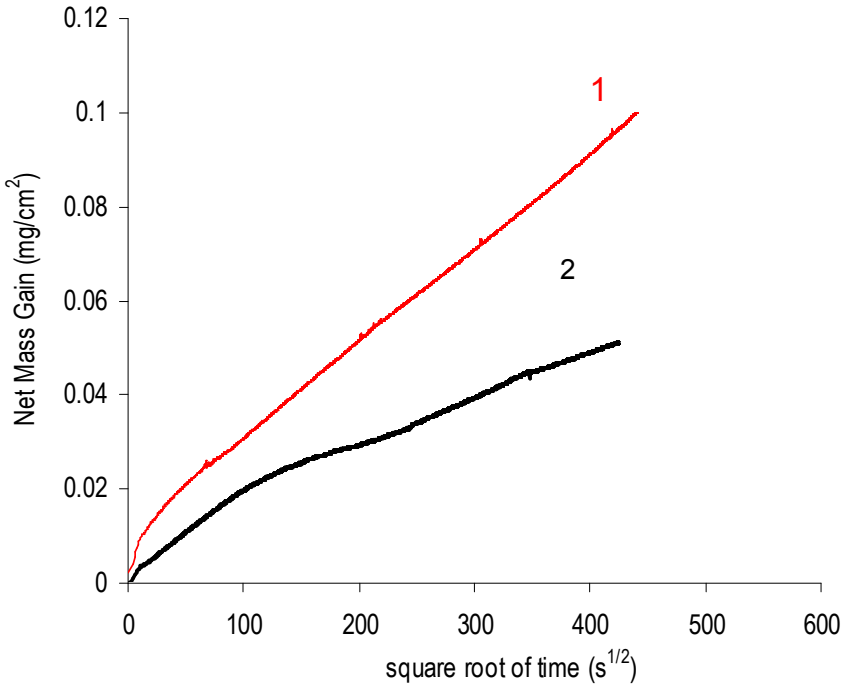

Fig. 3. Oxidation kinetics of samples tested at 600°C in synthetic air (1: without coating, 2: A350 sample)

Mechanical properties

Nanoindentation tests allowed determining the mechanical properties of the films. The obtained results are summarized in Table 4. The evolution of the nanoindentation curves depends on the processing temperature. The elastoplastic behaviour of the films was determined by the ratio of the elastic energy restored with unloading over the total energy of deformation. This ratio diminishes with increasing the deposition temperature (table 4). The calculated hardness and the rigidity of the films are also given in table 4. These values are very low compared to bulk alpha alumina. Maximum hardness and rigidity are obtained with the sample processed at 480 °C. On the other hand, the rigidity and the hardness of films processed at 700 °C are very low.

Fig. 4 presents surface SEM micrographs of scratches obtained on samples A350, B480 and C700 with increasing load. The obtained results highlight two scratch behaviours. Failure of coatings A350 and B480 is adhesive. The breaking pattern represents a brittle failure by cleavage without any plastic deformation. The coating processed at 700 °C is damaged as of the first scratching with a load of 30 mN. This coating has a very low cohesion but remains present on the surface of titanium alloy independently of the applied load.

Table 4: Mechanical properties of the coatings

	A350	B480	C700
Total energy [pJ]	451	991	59.1
Elastic energy [pJ]	265	337	9.75
Plastic energy [pJ]	185	654	49.3
Ratio elastic energy/total energy	0.59	0.34	0.16
Young modulus[GPa]	92 ± 8	155 ± 6	11.5 ± 2.8
Hardness [GPa]	5.8 ± 0.7	10.8 ± 0.8	1.1 ± 0.4

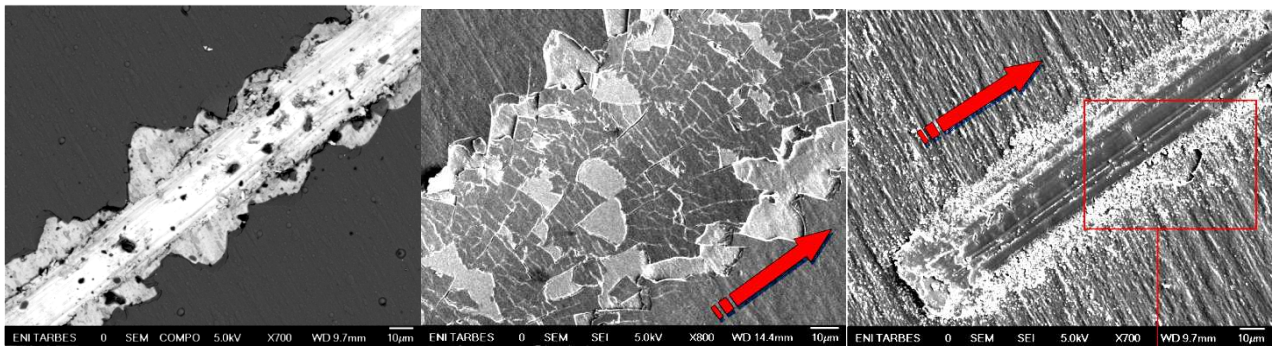

Fig. 4. SEM micrographs of the scratches: A350 (left), B480 (middle), C700 (right).

The adhesion of the coatings to the TA6V substrates was also estimated with a micro-tensile test under binocular. The percentage of coating scaled on the surface of the samples was determined by SEM image analysis (Table 5, Fig. 5). Moreover the shear stress to the coating/substrate interface was calculated with the model by Agrawal and Raj according to the damage feature of the coatings[18]. The failure of the films processed at 350 °C and at 480 °C is adhesive whereas that of the film deposited at 700 °C is cohesive. The maximum shear stress is reached for the coating processed at 350 °C.

Table 5: Percentage of failure and critical stress at the interface

Sample code	failure [%]	σ_e [MPa]	δ [µm]	λ [µm]	τ [MPa]
A350	17 %	1075	700	3.70	1249
B480	57 %	2026	880	14.34	610
C700	0 %	156	970	25.38	24

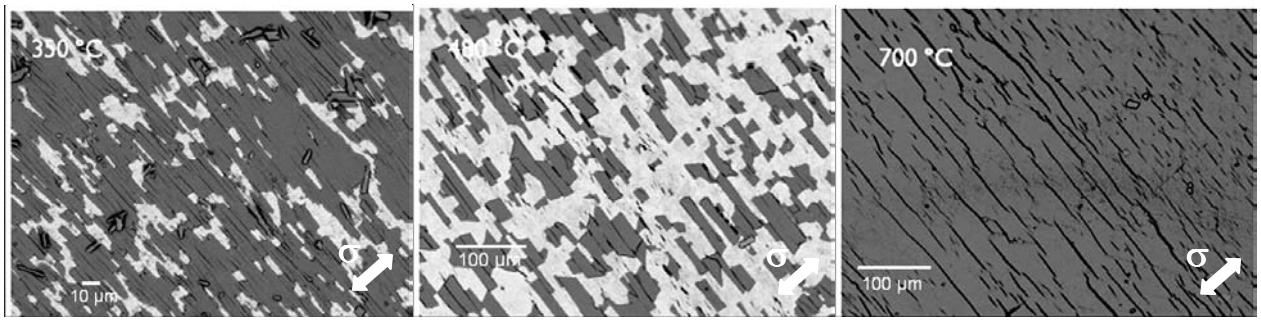

Fig. 5. SEM micrographs of the tensile samples near the fracture zone.

Conclusions

Aluminium oxide coatings were processed on TA6V titanium alloys by MOCVD from ATI at 5 Torr and different temperatures. Depending on the deposition temperature, these coatings are non-crystalline (350 °C, code A350 and 480 °C, code B480) or contain crystalline nanoparticles imbedded in an amorphous matrix (700 °C, code C700); they are composed of aluminium oxyhydroxide (A350) or alumina (B480, C700). An apparent kinetic law has been established in the range of conditions studied, leading to a representation of local deposition rates with an error lower than 20%. Voltammetry investigations revealed that sample B480 presents the lowest cathodic and anodic current densities. The surfaces of samples B480 and A350 are hydrophobic, with water contact angle of 103-106 degrees, in contrast to the high temperature one which is hydrophilic (water contact angle 48 degrees). Sample A350 presents significantly lower oxidation kinetics in dry air than the bare alloy. Maximum hardness and rigidity are obtained with sample B480. The coatings A350 and B480 present adhesive failure, in contrast to sample C700 which presents cohesive failure. Although preliminary, these results on barrier, mechanical and surface properties of MOCVD processed aluminium oxide films show promise for the implementation of such coatings in aeronautical components and more generally in various application domains.

Acknowledgments

The financial support of the Institut National Polytechnique de Toulouse through a Bonus Qualité Recherche is acknowledged.

References

[1] C.-J. Wang, Y.-C. Chang, Mat. Chem. Phys. 76 (2002) 151.
[2] J. D. Béguin, D. Samélor, C. Vahlas, A. N. Gleizes, J. A. Petit, B. Sheldon, Mat. Sci. Forum 595-598 (2008) 719.
[3] G. Boisier, M. Raciulete, D. Samélor, N. Pébère, A. N. Gleizes, C. Vahlas, Electrochem. Solid. State Let., 11 (2008) C55.
[4] A. Gleizes, M. M. Sovar, D. Samélor, C. Vahlas, Adv. Sci. Techn. 45 (2006) 1184.
[5] A. Gleizes, C. Vahlas, M. M. Sovar, D. Samélor, M. C. Lafont, Chem. Vap. Dep. 13 (2007) 23.
[6] A. M. Huntz, M. Andrieux, C. Vahlas, M. M. Sovar, D. Samélor, A. N. Gleizes, J. Electrochem. Soc. 154 (2007) P63.
[7] M. M. Şovar, D. Samélor, A. N. Gleizes, P. Alphonse, S. Perisanu, C. Vahlas, Adv. Mater. Res. 23 (2007) 245.
[8] M. M. Sovar, D. Samélor, A. N. Gleizes, C. Vahlas, Surf. Coat. Technol. 201 (2007) 9159.
[9] D. Samélor, M. M. Sovar, A. Stefanescu, A. N. Gleizes, P. Alphonse, C. Vahlas The Electrochemical Soc. Proc. Vol. 2005-09 (2005) 1051.
[10] D. Monceau, B. Pieraggi, Oxid. Met. 1998, 50, 477.
[11] W. C. Oliver, G. M. Pharr, J. Mat. Res. 19 (2004) 3.
[12] K. L. Mittal, Adhesion measurement of films and coatings : a commentary, Adhesion measurement of films and coatings, K.L. Mittal Ed., (1995), pp.1-13
[13] R. W. J. Morssinkhof, PhD thesis, University of Twente, 1991.
[14] R. Hofman, R. W. J. Morssinkhof, T. Fransen, J. G. F. Westheim, P. J. Gellings, Mat. Manuf. Proc. 8 (1993) 315.
[15] P. Kofstad, High Temperature Oxidation of Metals, Wiley, NY 1966.
[16] P. Kofstad, K. Hauffe, H. Kjollesdal, Acta Chem. Scand. 12 (1958) 259.
[17] A. M. Chaze, C. Coddet, J. Less Common Met. 157 (1990) 55.
[18] D. C. Agrawal, R. Raj, Acta Met. 37 (1989) 1265.